Histol Histopathol (2014) 29: 1477-1488
DOI: 10.14670/HH-29.1477

http://www.hh.um.es

Histology and Histopathology
Cellular and Molecular Biology

Correlation between 3D microstructural and 2D histomorphometric properties of subchondral bone with healthy and degenerative cartilage of the knee joint

Andreas Lahm[1,2], Richard Kasch[1], Heiko Spank[1], Christoph Erggelet[3], Jan Esser[1], Harry Merk[1] and Eike Mrosek[4,5]

[1]Section of Orthopaedic Research and Cell Biology, Department of Orthopaedics and Orthopaedic Surgery, Ernst-Moritz-Arndt University Greifswald, F.-Sauerbruch Str., Greifswald, [2]Kliniken Maria Hilf Mönchengladbach, Academic Teaching Hospital of the RWTH Aachen, Mönchengladbach, [3]Arthrose Clinic Zürich, Zürich, [4]Department of Trauma and Reconstructive Surgery, Schwarzwald-Baar-Klinikum Villingen-Schwenningen, Villingen-Schwenningen and [5]Cartilage and Connective Tissue Research Laboratory, Department of Orthopaedic Surgery, Mayo Clinic College of Medicine, Rochester, MN, USA

Summary. Cartilage degeneration of the knee joint is considered to be a largely mechanically driven process.

We conducted a microstructural and histomorphometric analysis of subchondral bone samples of intact cartilage and in samples with early and higher- grade arthritic degeneration to compare the different states and correlate the findings with the condition of hyaline cartilage. These findings will enable us to evaluate changes in biomechanical properties of subchondral bone during the evolution of arthritic degeneration, for which bone density alone is an insufficient parameter.

From a continuous series of 80 patients undergoing implantation of total knee endoprosthesis 30 osteochondral samples with lesions macroscopically classified as ICRS grade 1b (group A) and 30 samples with ICRS grade 3a or 3b lesions (group B) were taken.

The bone samples were assessed by 2D histomorphometry (semiautomatic image analysis system) and 3D microstructural analysis (high-resolution micro-CT system). The cartilage was examined using the semiquantitative real-time PCR gene expression of collagen type I and II and aggrecan.

Both histomorphometry and microstructural and biomechanical analysis of subchondral bone in groups A and B consistently revealed progressive changes of both bone and cartilage compared with healthy controls.

The severity of cartilage degeneration as assessed by RT PCR was significantly correlated with BV/TV (Bone Volume Fraction), Tb.Th (Trabecular Thickness) showed a slight increase.

Tb.N (Trabecular Number), Tb.Sp (Trabecular separation) SMI (Structure Model Index), Conn.D (Connectivity Density) and DA (Degree of Anisotropy) were inversely correlated.

We saw sclerotic transformation and phagocytic reticulum cells. Bone volume fraction decreased with an increasing distance from the cartilage with the differences compared with healthy controls becoming greater in more advanced cartilage damage.

The density of subchondral bone alone is considered an unreliable parameter for classifying changes evolving over time. The progressive damage of subchondral bone seen in the present study correlates well with cartilage changes. Trabecular orientation is also impaired, which explains the changes in biomechanical parameters and the inadequate load transfer and excessive loading of cartilage. Besides subchondral bone density, which in turn correlates with cartilage thickness, other parameters such as structure model index and grade of anisotropy best reflect mechanical properties such as Young modulus, compressive strength, tensile stress, and failure energy.

However, it remains unclear whether the mechanical interaction of the mineralized subchondral tissues with articular cartilage works vice versa. The possibility of a biochemical signalling from the degenerating cartilage via the synovial fluid and bone- cartilage crosstalks via subchondral pores may indeed explain a certain depth-

Offprint requests to: Prof. Dr. med Andreas Lahm MPH, Section of Orthopaedic Research and Cell Biology, Department of Orthopaedics and Orthopaedic Surgery, Ernst-Moritz-Arndt University Greifswald, F.-Sauerbruch Str., D-17475 Greifswald, Germany. e-mail: alahm@uni-greifswald.de

dependency of subchondral bone changes.

Key words: Microstructural and histomorphometric properties, Subchondral bone, PCR, Cartilage degeneration

Introduction

The capacity of hyaline cartilage to undergo regeneration and repair is limited and has not yet been fully elucidated, and our knowledge of the etiology and pathogenesis of arthritis and its progression is also far from being complete. Specifically, the role of subchondral bone remains to be definitely clarified - particularly with regard to whether it initiates the degenerative process or is affected by it secondarily.

The most discussed topic is that of subchondral sclerosis. Since the publication of Radin et al. (1986), numerous investigators have addressed different aspects of this issue. The group focused on the role of subchondral bone as an effective shock absorber and hypothesized that sclerosis would lead to a stiffer subchondral structure with a decreased shock-absorbing capability, thereby increasing the stress in the overlying cartilage and initiating its deterioration.

The origin hypothesis assumed that, because articular cartilage and subchondral bone are viscoelastic, the joint ends deform when loaded, and this viscoelasticity maximizes the contact area under the load and minimizes stresses and was concisely determined later. The mechanical capacity to withstand tension or shear stresses that occur at the edges of the joint contact regions is limited.

Splitting or fibrillation caused by tension or shear stresses that occur at the edges of the joint contact regions are exacerbated by inhomogeneities in the density and stiffness of the underlying subchondral bone. The latter would cause cartilage to deform more in regions over-lying less dense parts of the subchondral plate than in regions over denser portions of the plate. Sclerosis and bone matrix mineralization are related, as the increase in bone volume fraction has been hypothesized to result from bone adaptation in response to decreased mineralization. Burr and Gallant (2012) stated that sclerosis and accelerated remodelling in OA are not inconsistent observations, but simply reflect different temporal stages of disease or different spatial locations, or both.

The remodelling of bone, -with its intrinsically higher capacity for healing than cartilage -is mainly regulated by the balanced processes of osteoclast-mediated bone resorption and osteoblast-mediated bone formation. Dysfunction of this balance leads to dysregulated bone tissue remodeling, which might result in excessive bone loss or extra bone formation (Zhang et al., 2012). Previous studies have demonstrated that early subchondral bone loss is followed by increased bone density and OA progression.

Another aspect that is not yet fully understood is whether thickening of the subchondral plate also has any causative effects. After all, experimental results suggest that cartilage degeneration begins in areas overlying thickened portions of the subchondral plate and is absent where the plate has normal thickness.

Investigations in alternative animal models such as the canine groove model or the canine anterior cruciate ligament transection model (Marijnissen et al., 2002, Liu et al., 2003; Sniekers et al., 2008) revealed a considerable reduction in the thickness of the subchondral plate, which was associated with increased articular cartilage destruction and reduced synthesis of glycosaminoglycans.

In contrast, Raudenbush et al. (2003) did not find a correlation between cartilage degeneration and subchondral thickness; however, it must be noted that steep stiffness gradients are not only a result of subchondral thickness but also of several other parameters measured

The situation is also unclear with regard to cellular signalling. Growth factor β, insulin-like growth factor, interleukin (IL)-1, IL-6 and prostaglandin E2 protein are known to modulate chondrocyte proliferation and differentiation and matrix synthesis. Again, release of these factors both results from and stimulates bone remodelling.

Proteoglycan content determines stiffness (Kempson et al., 1973) and collagen fibrils provide resistance against cartilage deformation. These molecules, which form huge aggregates and have a significant hydration shell, are responsible for the weight-bearing capacity of healthy articular cartilage. This requires the maintenance of a delicate balance. On the one hand there is the intrachondral swelling pressure that keeps the cartilage "stretched" and results from osmotic pressure and electrostatic repulsion between neighboring glyco-saminoglycans and polysaccharides on proteoglycans, and on the other hand there is the collagen network to provide resistance against deformation. Investigations during progression of OA and the observed structural changes show that the release of sulfated glycosaminoglycan (GAG), the degradation of type II collagen, and the overproduction of cytokines are central pathophysiological events in OA. The course of the disease is related to different complex pathways and mechanisms, including excessive production of proteolytic enzymes such as the aggrecanases and MMPs. Chondrocytes can modulate their functional capacity in response to loading but their ability to do so is limited compared with bone.

In the current study we aimed to assess changes in articular cartilage and correlation between the expression of collagen type I and II in relation to other ECR components in different cartilage layers, as well as the relation to stereological measures of subchondral bone structure during the progression of early towards advanced osteoarthritic degeneration and to analyze the associated immunohistochemical changes in tissue

metabolism. Therefore, with the help of immunohistochemistry, real-time polymerase chain reaction (RT-PCR) and quantitative RT-PCR we investigated human knee joint cartilage tissue for its collagen type I and II and aggrecan content and correlated it with 3D microcomputed tomography and 2D bone histomorphometry of the underlying subchondral bone.

Materials and methods

From a continuous series of 80 patients undergoing implantation of total knee endoprosthesis osteochondral samples (one sample per patient) with lesions macroscopically graded as ICRS grade 1b (group A; with recognizable cracks and fissures) and with ICRS grade 3a or 3b lesions (group B) were taken from the femoral condyles.

To standardize the following examinations in these groups we identified 30 samples each with Collins and McElligott histopathological grading (Miosge et al., 2004) of I and III respectively with 4,8 and 9,2 points (groups A and B respectively) in the "histological-histochemical grading system" (HHGS) for osteoarthritis scores, the modified "Mankin Score" (Ehrlich et al. 1986).

The samples were drawn at a right angle from as deep as the subchondral bone. The patients in group A ranged in age from 56-73 years (average: 64 years, 18 women, 12 men), those in group B from 56-74 years (average: 65 years; 19 women, 11 men). Twenty control biopsies with macroscopically healthy cartilage (ICRS grade 0) were taken from the same region, 12 of these taken during an ACI (autologous chondrocyte implantation), 7 during endoprosthesis implantation (mainly after extra-articular resection of the distal femur or without proximal tibia and reconstruction with a tumour endoprosthesis) and 1 during major amputation (age: 26-68 years, average: 47 years; 10 women and 10 men). We excluded patients with rheumatoid arthritis, ankylosing spondylitis, psoriasis or similar arthritides, and malignancies or infections with inflammatory arthritides. The control group included subjects with a Collins and McElligott histopathological grading of 0 and normal articular cartilage in the "histological-histochemical grading system" (HHGS) for osteoarthritis.

Approval was given by the institutional review board, and informed consent was obtained from each patient.

After tissue prefixation and decalcification in EDTA the sections were dehydrated, and Epon (1:1) embedded (Epon 812, Fa. Carl Roth GmbH, Karlsruhe). Formalin fixation, slicing into semithin sections (5 µm), and paraffin staining were performed according to standardized procedures (Lahm et al., 2006). All histological sections (x50) with safranin O (Chroma-Gesellschaft Schmid & Co), PAS (Chroma-Gesellschaft Schmidt & Co) Alcian blue (Merck), and immunohistochemical stains were examined with light and polarization microscopy, photographed (Axioskop, Zeiss, Oberkochen, Germany and Kodak Elite 400) and scanned.

Monoclonal mouse antibodies (anti-human collagen I and collagen II) were used for the immunohistochemical analysis (Immunodiagnostika und Biotechnologie, Berlin, Germany). Hyaluronidase digestion was performed to identify collagen fibers (10.000 U Hyaluronidase/ml; 37°C for 2.5 hours; Sigma Chemicals, St. Louis, USA). Enzyme activity was stopped by rinsing three times with PBS buffer.

The cryo-sections were then pre-incubated at room temperature for an hour in a humid chamber with 1% BSA. After suctioning off the BSA, primary antibody was added to each object (ca. 50μl/object). The antibody added (fluorescein-conjugated secondary antibody) was diluted 1:100 in BSA.

PCR

For the actual measurements 20 samples of healthy cartilage and 30 samples with macroscopically ICRS grade 3a or 3b lesions were used.

RNA extraction

According to Oncoscreen instructions, Baelde et al. (2001) and Ruettger et al. (2011) RNA isolation from human cartilage tissue was performed. For each sample, 0.03 cm^3 of frozen material from each patient was minced and mixed with 5 ml of Trizol (Invitrogen) and 5 μl of glycogen (Invitrogen). With the help of a syringe and various disposable cannulas (sizes 21 and 14, Fisher Scientific) each sample was then homogenized. 1 ml chloroform (Roth) was added, and the suspension was mixed thoroughly and then centrifuged for 10 minutes at 13200xg. RNA was precipitated with isopropanol (Roth). The pellet was washed twice with 70% ethanol (Roth), dried and then placed in 45 μl of highly purified water (Invitrogen).

Identification of RNA concentration

The RNA concentration was measured with a nanophotometer (Implen).

Characteristics of analytical primers

The sequence for the reference gene HPRT1 corresponded to that used by Vandesompele et al. (2002). COL1A1 and COL2A1 sequences corresponded to those used by Miosge et al. (2004). Analyzing the aggrecan content a new design of primers was created usable for human cartilage (see Table 1). For all primers searches for similar sequences were performed using BLAST. It was also confirmed that for all amplicons there were exon overlapping primers.

Primer survey and gel electrophoresis

The amplicons HPRT, COl1A1, COl2A1 and Agg for PCR were checked using classical PCR with the test essays c60095/1 and c60095/2. For this, RNA was extracted, reverse transcription was performed and cDNA was produced, 2 μl of which were used for the classical PCR. PCR products were placed on 1.2% agarose gel. All amplicon bands lay in the expected range with no sign of double bands.

The quality of extracted RNA samples was tested by adding 350 ng of RNA per track to 1.2% agarose gel and separating at 130V for 60 min.

Reverse Transcription

RNA samples were converted into cDNA (10 ng/μl).

Quantitative PCR

Beginning with a final sample of 25μl we added the following: 12.5 μl 2x QuantiFast SYBR Green PCR Master Mix (Qiagen), 6.5 μl RNAse-free water (Qiagen), 1 μl primer mix (6 mM) and 5 ng cDNA. For each gene being measured, 4 dilution series were made.

ABI 7500 (Applied Biosystems) was used for quantification

After initial denaturation at 95°C, cDNA products were submitted to 40 PCR amplification cycles (5 min). This included denaturation (95°C for 15 seconds) and then extension/annealing (60°C for 60 seconds). Validity of the PCR results was verified by sequencing and melting curves (Fig. 1).

2D Bone sectioning and histomorphometry

The bone sections were assessed in an Axioskop microscope (Carl Zeiss AG, OberkochenGermany) at 200-fold magnification and analyzed using a specialized software tool of the Kodak Elite 400 semiautomatic image analysis system (Carl-Zeiss Jena). The technique used was a modification of the technique of Panula et al. (1998) that has been used by several groups before (Lahm et al., 2006, Zhang et al., 2011). In brief, a line of defined length was drawn with the cursor distal to the last complete chondrocyte row and stored. This line was automatically shifted in parallel in 65 steps. In each position, the software determined the sum of all segments of the line on mineralized structures and the number of trabecles intersected by the line. These data were stored for each line position, or distance from the baseline.

The following histomorphometric parameters were measured or calculated from measurements: Trabecular bone volume (%; number of pixels representing the bone area divided by the number of pixels representing the combined bone and marrow area) Trabecular number per unit, Trabecular thickness (mm) Osteoid thickness (μm) Osteoid surface (%) Osteoid volume (%) Osteoblast number per unit Osteoblast surface (mm^2/cm^3) Osteoclast number per unit Osteoclast surface (%) Total eroded surface (%) and Total erosion depth (μm)

3D Microcomputed Tomography and stereology

The embedded bone biopsies were fixed in formalin and scanned in a desktop Micro CT scanner (µCT-40, Scanco Medical, Bassersdorf, Switzerland; http://www.microct.com) at an isotropic voxel size of 21 µm (70 kVp, 114 µA, 500 projections per 180 degrees, 300ms integration time). A beam-hardening correction algorithm was applied to all scans.

Image processing included Gaussian filtering (sigma=0.8, support=1) and segmentation with a constant threshold value as in this setting discrimination between bone and other tissues is important.

The length of the bone cylinder was scanned with up to 2000 transverse slices per biopsy, each slice consisting of 1024×1024 pixels. The virtual-slicing direction perpendicular to the main axis of the biopsy is recommended to achieve the high resolution (Thomsen et al., 2005)

The following parameters were measured or calculated from measurements:

BV/TV: Bone Volume Fraction, Tb.N: Trabecular Number, Tb.Th: Trabecular Thickness, Tb.Sp: Trabecular separation, SMI: Structure Model Index, Conn.D: Connectivity Density, DA: Degree of

Table 1. Description of the designed primers and probes designed for PCR.

Gene amplicon identification	Identification	Accession number	Amplicon length	Sequence Forward/Reverse	Annealing temperature
HPRT I	HPRT496F	NM_000194	94bp	TGA CAC TGG CAA AAC AAT GCA	TM=50.5°C
HPRT496A	HPRT589R			GGT CCT TTT CAC CAG CAA GCT	TM=54.4°C
Collagen type I	Col1A1_81F	NM_000088	256bp	TCC CCA GCC ACA AAG AGT C	TM=53.2°C
Col1A1A	Col1A1_336R			CGT CAT CGC ACA ACA CCT	TM=50.3°C
Collagen type II	Col2A1_2976F	NM_033150	149bp	CTC CTG GAG CAT CTG GAG AC	TM=55.9°C
Col2A1A	Col2A1_3124R			ACC ACG ATC ACC CTT GAC TC	TM=53.8°C
Aggrecan	Agg32512F	NC_000015	170bp	ACT TCA GAC CAT GAC AAC TCG	TM=52.4°C
Agg32512A	Agg35067R			ACA CGG CTC CAC TTG ATT CTT	TM=52.4°C

Anisotropy

Bone Volume Fraction (BV/TV) was computed using voxel counting. Trabecular number (Tb.N*), thickness (Tb.Th*) and separation (Tb.Sp*) were obtained by measuring 3D distances directly in the trabecular network. The structure model index, which is a model of predominant shapes in the bone structure, (plate-like to rod-like) was determined by a differential analysis of the triangulated bone surface (Hildebrand and Rüegsegger, 1997). As with Tb.Th, Tb.Sp was only determined in voxels not assigned to bone (i.e., voxels with attenuation values below the defined threshold). SMI is an estimation of the plate-like or rod-like (cylindrical) characteristics of the SB structure. The ideal plate and cylindrical architectures have SMI values of 0 and 3 respectively (Ding et al., 2002). A rod-like trabecular bone structure has higher mechanical strength than a plate-like structure (Ding et al., 2003).

The degree of anisotropy is defined as the ratio between the two eigen values, that is the ratio of eigen value of primary direction divided by eigen value of tertiary direction (Goulet et al., 1994).

Statistics

Comparison of the mean values of 3D micro-computed tomography and 2D bone histomorphometry parameters of the underlying subchondral bone was performed using a paired samples t-test. For each parameter, differences between groups were tested for significance using analysis of variance (one-way ANOVA). Correlation between the RT-PCR expression values and bone parameters was calculated using Pearson correlation with results considered significant at $p>0.05$.

Results

Results of ΔCt method

Differences between target and reference genes were calculated in the first step using the classical ΔCt Method manner (Vandesompele et al., 2010; Miosge et al., 2004) with target genes COL1A1, COL2A1 and Agg and HPRT I acting as reference gene.

To calculate the ΔCt values a linear transformation following the equation $2^{-\Delta Ct}$ was performed. A calibrator curve was obtained by the correlation of the ΔCt values (threshold cylces) with the dilution series of the house keeping genes.

The relation of the values for the genes Col1A1, Col2A1 and Agg to the reference gene is shown in Table 2 with an example for collagen type II demonstrated in Fig. 2.

In group A a slightly increased color intensity was found for collagen II in deeper layers, suggesting a persisting but initially still intact repair process. Loss of this repair mechanism at the surface was reflected in a significant decrease in collagen II content, leading to an early reduction in total collagen II. A significant increase in collagen type I was found in group B, but it is generally expressed in earlier stages with a pronounced expression of collagen type I mRNA.

Physiologic proteoglycan content near the surface in healthy cartilage is low in all mammalians. In the transitional zone directly beneath the surface, safranin O

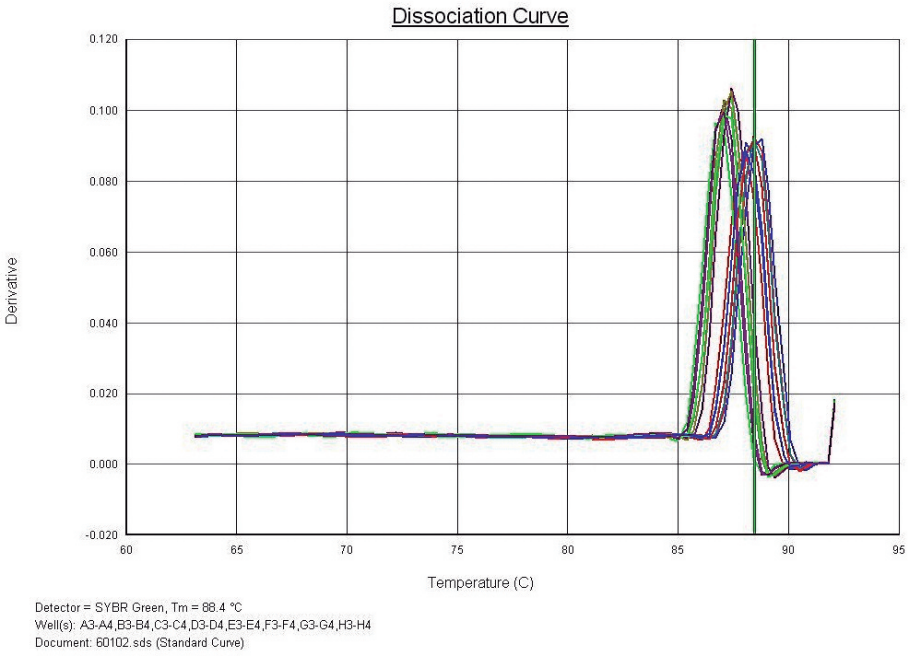

Fig. 1. Melting curves for collagen II and aggrecan genes. The first peak at 86°C (aggrecan) and the second at 88°C (collagen II) show that no other transcripts were amplified in the PCR.

stainability is slightly higher but still less intense than in the deeper, radial zone (Fig. 3). In contrast, markedly decreased safranin O staining intensity was observed in the radial zone and less reduced intensity in the transitional zone with loss of zonal anatomy in 40% of the specimens in group A and all specimens in group B. These changes in staining intensity were accompanied by typical OA changes such as cell-clustering, hypocellularity or surface erosion (Fig. 4), as well as a relative thickening of the calcified cartilage with an increase of the distance between tidemark and subchondral bone. Aggrecan turnover in damaged areas showed significant variation but tended to be lower than in healthy cartilage and correlated only weakly with the

Table 2. Ratios between expression values for the genes Col1A1, Col2A1 and Agg and the reference gene and calculation of the ΔCt values (means and quotients between expression values for the genes Col1A1, Col2A1 and Agg and the reference gene.

	Col1A1 $2^{\Delta Ct}$	Col2A1 $2^{\Delta Ct}$	Agg $2^{\Delta Ct}$
Control (mean)	0.017	0.0023	0.0092
Degenerative Group A (mean)	0.112	0.0009	0.0056
Quotient of ΔCt values			
Group A ·/· Control	6.6	0.39	0.61
Degenerative Group B (mean)	0.357	0.00044	0.0048
Quotient of ΔCt values			
Group B ·/· Control	21	0.19	0.52

Table 3. Bone histomorphometric parameters (Mean±SD) of groups A (4.8 in HHGS) and B (9.2 in HHGS) and in controls (=healthy control specimens).

Parameter	A (ICRS 1)	B (ICRS 3a/3b)	Control
Trabecular Bone Volume (%)	46±4.1	55±2.9	43±3.8
Trabecular Number	4.6±0.6	3.9±0,6	4.9±0.4
Trabecular Thickness (mm)	0.114±0.009	0.127±0.007	0.114±0.006
Osteoid Thickness (μm)	4.7±0,7	5.0±0.6	4.9±0.4
Osteoid Surface (%)	7.0±1.2	7.9±1.1	6.8±0.8
Osteoid Volume (%)	0.6±0.2	0.8±0.2	0.7±0.2
Osteoblast Number	129±40	171±20	117±31
Osteoblast Surf. (mm^2/cm^2)	2.0±0,7	2.5±0.8	1.9±0.5
Osteoclast Number	19±5	20±6	16±5
Osteoclast Surface (%)	0.9±0.4	1.0±0.3	0.7±0.3
Total eroded Surface (%)	6.9±1.3	7.5±1.4	6.8±1.0
Total Erosion Depth (μm)	5.1±0.8	6.1±0.8	4.8±0.6
Subchondral bone plate thickness (mm)	0.51±0.09	0.67±0.12	0.61±0.11

Fig. 2. Quantitative real-time PCR: curves for collagen II (healthy cartilage) with Ct values at 19 (second group of curves, cDNA 3, 4 and 7) and collagen II (group B) with Ct values at 15 (first group of curves, cDNA 8, 9 and 10). Calculation of collagen II content based on ΔCt value.

HHGS classification into controls and groups A and B (Table 2) or with safranin O staining intensity representing proteoglycans.

Table 3 shows the results for the different bone-structure parameters determined by 2D bone histomorphometry. There was a significant increase in the trabecular bone volume (comparable with bone volume fraction in 3D analysis) and a decrease in the trabecular number in group B. These are the most important parameters for which mostly non-significant tendencies were found in group A. The osteoblast number also increased significantly in group B, while the osteoclast number showed a tendency to increase in both groups. Especially at the edges of damaged zones we also found an increase in phagocytic-histiocytic reticular or other inflammatory cells. Osteoid Thickness and Osteoid Volume showed a slight decrease in the early arthritis group A in the 2-D examinations to increase non-significantly in group B representing an overlying cartilage graded ICRS 3a or 3B with an average HHGS score of 9.2 points.

3D parameters estimated from 3D μCT have been plotted in Table 4 with a significant increase in the Bone volume fraction and a decrease in the Trabecular Number, Connectivity Density, Degree of Anisotropy and Structure Model Index in group B as the most important parameters with mostly non-significant tendencies in group A.

The severity of hyaline cartilage degeneration based on a RT PCR increase of Col1A1 was significantly correlated with BV/TV ($P<0.001$) and inversely correlated with Tb.Sp ($P<0.001$), SMI ($P<0.001$),

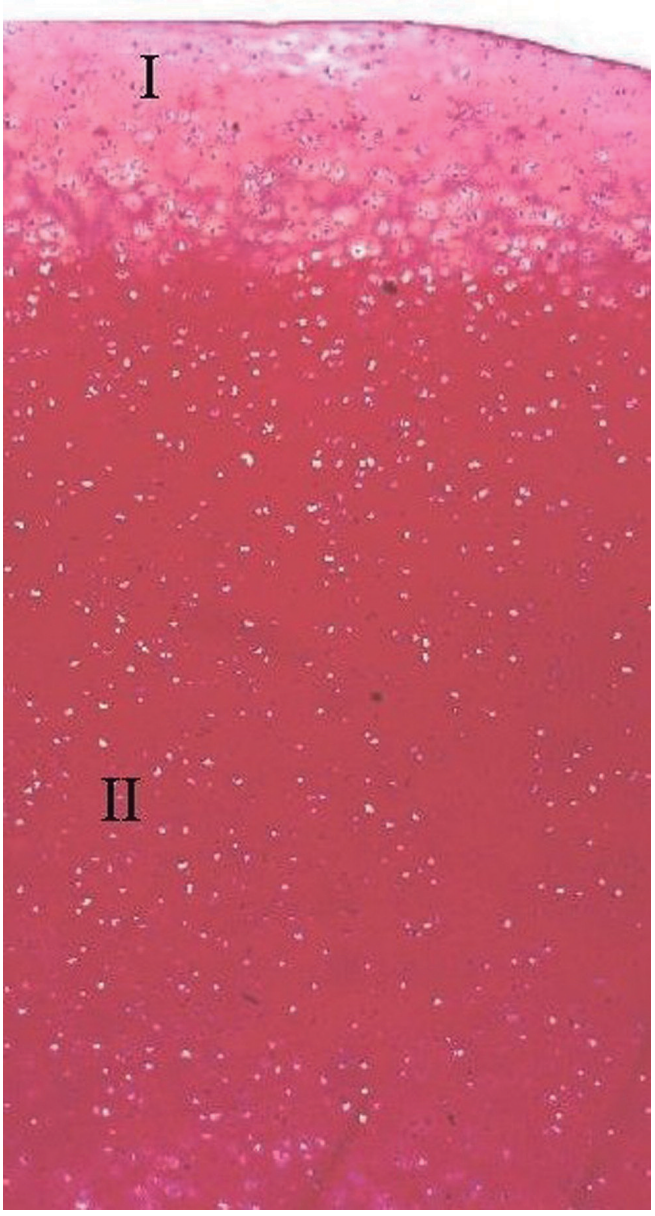

Fig. 3: Safranin O of healthy hyaline cartilage with intact zonal formation, high staining intensity and uniform cell distribution; I: Transitional zone; II: Radial zone. x 50

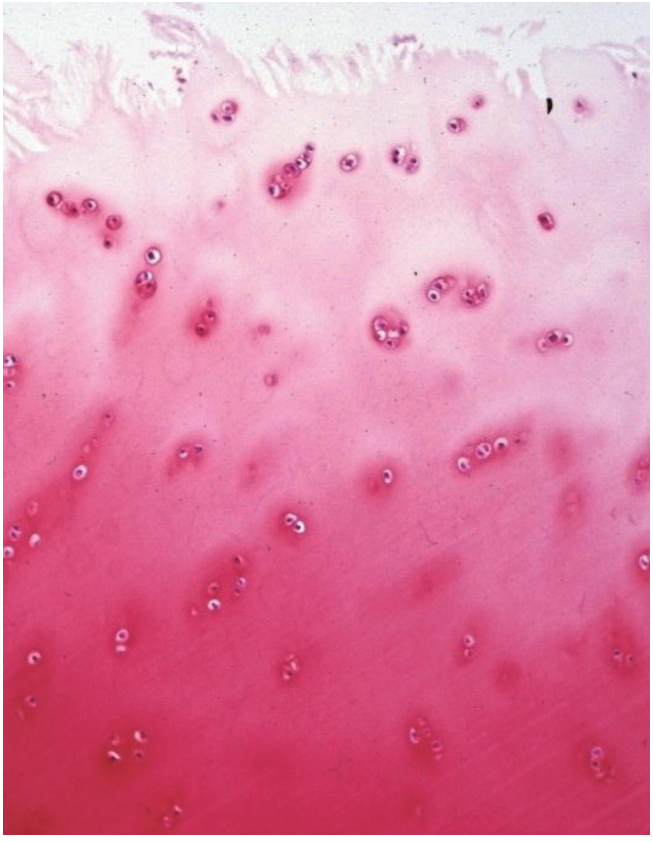

Fig. 4 Safranin O representing cartilage damage with cell-clustering, hypocellularity, surface erosion, and a decrease in staining, especially in the superficial and transitional zones as a result of abnormal cellular proteoglycan production. x 50

Conn.D (P<0.001) and DA (P<0.001) and vice versa with the decrease of Col2A1 (Table 5) with slightly weaker correlation, as we found a 5 fold down-regulation of collagen II but a more than factor 20 expression relation in Col1A1 both in group B compared with the control group. In group B the greatest Bone Volume Fraction (BV/TV) and Tb.Th were found in specimens in whom the ICRS grade 3a or 3b cartilage lesions were found in more peripheral (external as well as internal) areas of the medial condyle and in the internal area of the lateral condyle.

The slight decrease in the Degree of Anisotropy in group A was accompanied by a high standard deviation indicating that the decrease is not uniformly distributed in all directions, as the primary degree of anisotropy decreases by 29% in this group. These findings suggest that already in group A, the subchondral bone is less organized with trabeculae orientated less well to the main loading direction of the femoral condyle.

However, in the early osteoarthritis group A, both in 2D- and 3D- measurements in general showed that quite a high standard deviation was found, indicating an incoherent appearance of the subchondral bone in this group.

Corresponding parameters in 3D microcomputed tomography and 2D bone histomorphometry showed a high correlation, such as Bone volume fraction (3D) and Trabecular Bone Volume (2D) both for groups A and B and the difference in comparison to the control group (r=0,84 and r=0,95 respectively) as it was also demonstrated that on average the 2D bone histomorphometry estimated similar or slightly lower changes of values than those obtained from 3D microcomputed tomography (Tables 3 and 4). Concerning correlation between 2D and 3D examinations Trabecular Thickness is an exception as the significant increase of more than 10 % in the 2D measurement in group B was only accompanied by a non significant slight increase in 3D microcomputed tomography. Subchondral bone plate thickness decreased in group A by 17.2% and increased in group B by 10.2% (Table 3).

Interestingly, the bone volume fraction in 3D-measurements (not measured in 2D) decreased with an

Table 4. Summary of the 3D microstructural properties (mean ± SD) of subchondral bone in the three groups.

Parameter/Group	A (ICRS 1)	B (ICRS 3a/3b)	Control
Bone volume fraction (%)	28.3±10.4	38.3±7.1	26.2±8.5
Trabecular thickness (μm)	170±29	171±23	168±14
Trabecular Number (mm^{-1})	1.20±0.81	1.02±0.31	1.32±0.30
Structure Model Index (-)	1.02±0.54	0.84±0.29	1.19±0.39
Connectivity densitiy (mm^{-3})	5.92±1.45	4.64±1.19	6.45±1.33
Degree of anisotropy (-)	6.21±1.95	4.35±0.98	6.63±1.22
Trabecular separation (μm)	511±47	486±43	523±36

Table 5. Pearson´s correlation (with P< 0.001) of OA severity measured by RT-PCR and structural parameters of the underlying subchondral bone.

Parameter 3D/Group	Col1A1 $2^{\Delta Ct}$	Col2A1 $2^{\Delta Ct}$	Agg $2^{\Delta Ct}$
Bone volume fraction (%)	0.82	- 0.70	- 0.48
Trabecular thickness (μm)	0.22	- 0.26	-0.32
Trabecular Number (mm -1)	- 0.68	0.60	0.39
Structure Model Index (-)	- 0.73	0.65	0.58
Connectivity densitiy (mm -3)	- 0.71	0.61	0.49
Degree of anisotropy (-)	- 0.65	0.60	0.49
Trabecular separation (μm)	- 0.70	0.60	0.53
Parameter 2D			
Trabecular Bone Volume (%)	0.72	- 0.65	- 0.42
Trabecular Number	-0.61	0.58	0.37
Trabecular Thickness (mm)	0.53	- 0.50	- 0.40
Osteoid Thickness (μm)	0.10	- 0.18	-0.19
Osteoid Surface (%)	0.62	-0.53	-0.45
Osteoblast Number	0.80	-0.71	-0.54
Total Erosion Depth (μm)	0.65	-0.59	-0.51

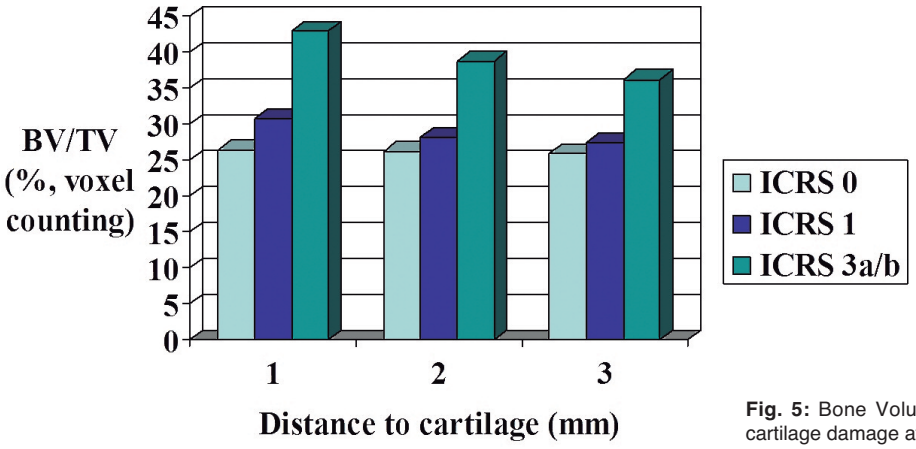

Fig. 5: Bone Volume Fraction (ordinate) for different grades of cartilage damage at different distances from cartilage (abscissa).

increasing distance from the cartilage, and the difference to healthy controls was greater in more advanced cartilage damage (Fig. 5). That means that the decrease in mineralization, corresponding to the bone volume fraction, was highest close to the cartilage, as the difference in BV/TV between the groups ICRS 0 and ICRS 3a/3b groups was highest at a depth of 1mm beneath the cartilage (Control 26.4% versus 43.0% at 1 mm and 26.0% versus 36.2% at 3 mm). Concerning all other bone parameters, differences between levels decreased within the groups with progression of cartilage changes, meaning that more severe OA was associated with a deeper extent of changes in bone architecture

Discussion

The biomechanical, immunological, and biochemical processes involved in the pathogenesis of osteoarthritis are complex and not yet fully understood. What is undisputed is that the subchondral bone plays a central role in OA. In individuals with OA, the balanced process of bone formation and resorption is disturbed qualitatively and quantitatively. This alters the mechanical properties, which, as has long been known, will ultimately lead to an increased density of the subchondral mineralization zone and the trabeculae underneath. As a result, the subchondral bone becomes stiffer and loses its shock absorber function, a property first ascribed to subchondral bone several decades ago. Several biomechanical parameters have been established to assess these changes.

It is surprising that the term subchondral bone is not used consistently but instead may subsume different anatomical structures.

According to Duncan et al. (1987) and Burr and Gallant (2012), the zones of calcified cartilage and the underlying corticalized bone layer can be regarded as a functional unit in several respects.

One reason is that this calcified cartilage, which separates the subchondral cortical bone from the non-mineralized articular cartilage at the tidemark, contributes to the biomechanically important sclerosis observed in advanced OA. This tidemark consists of 8-10 layers of collagen fibrils arranged in a thick bundle.

We know that besides subchondral bone plate density (which significantly correlates with the anatomic cartilage thickness (Akiyama et al., 2012)) the structure model index as well as the Degree of Anisotropy and the Connectivity best predict the mechanical properties of cancellous bone such as Young Modulus, Compressive Strength, Tensile Stress and Failure Energy (Ding et al., 2002, 2003).

Our study shows that there is a very good correlation between 3D microcomputed tomography and 2 D bone histomorphometry of the underlying subchondral bone. Histomorphometry based on a 2D plate model enables good estimates of the trabecular number from the ratio between trabecular surface and bone volume fraction, whereas the unbiased and assumption-free quantification of the so-called connectivity (number of trabeculae per volume) in 3D imaging systems is based on a topological approach. This is typical for sometimes somewhat puzzling comparisons, as relationships between parameters are of an empirical rather than a theoretical nature (Thomsen et al., 2005). The same group also found an excellent correlation between the Structure model index derived from 3D μCT and the trabecular bone pattern factor in 2D sectioning and stereology, again also confirming that the SMI is not the 3D representation of the trabecular bone pattern factor, as the SMI is dimensionless, whereas the trabecular bone pattern factor has the dimension mm^{-1}, which on the other hand is the dimension of the Trabecular Number (Tb.N) in the 3D system.

Topographically, the greatest Bone Volume Fraction (BV/TV) and Tb.Th were found in more peripheral (external as well as internal) areas of the medial condyle and in the internal area of the lateral condyle.

In most specimens we found advanced degenerative cartilage changes in these areas of the condyles compared with the surrounding tissue.

In addition, cellular inflammatory-like infiltrations were also more common in these areas.

Sokolove and Lepus (2013) have suggested that bone changes represent a local inflammatory process at the bone-cartilage interface and that this interaction forms a functional unit which, when disturbed by damage or inflammation, is involved in the initiation of OA. This group also observed bone lesions at the time of total joint arthroplasty representing low-grade inflammation, accompanied by findings of localized infarction as demonstrated by vascular leak and local fibrinoid reactions with thrombus inclusions. One obvious weakness is the late stage at which these lesions were obtained. However, both cellular necrosis and vascular leak may provide a source of DAMPs capable of contributing to ongoing inflammation.

The topographic variation in Tb.Th was so large that the increase in ICRS 3a/3b specimens was not significant. In contrast, the Structure model index, Connectivity density and the degree of anisotropy decreased in 3D patterns, indicating the loss of mechanical properties. This is in agreement with the results of Cox et al. (2012) who also found a decrease in bone matrix mineralization. The separation of the trabeculae compromises the robustness of the bony scaffold in addition to the above mentioned change in elasticity and the resulting loss of support for the overlying cartilage.

Bobinac et al. (2003) found bone matrix mineralization to correlate with the degree of degeneration of the overlying cartilage and to be changed most markedly directly underneath the cartilage.

The observations, however, do not allow to decide whether the association between subchondral bone loss and cartilage damage is part of a pathogenetic sequence,

or simply rep-resents non-causal and independently occurring changes in bone and cartilage during the development of OA. Therefore, it remains controversial whether these bony changes are a cause or consequence of other changes in osteoarthritis.

Especially in some animal models, alterations of the subchondral bone have been observed to precede cartilage changes (Lahm et al., 2006; Quasnichka et al., 2006), sometimes demonstrating subchondral bone changes very early after induction of disease. Other reports suggest that cartilage changes may occur first and subsequently might influence subchondral bone density and other parameters (Bobinac et al., 2003; Burger et al., 2007). However, another set of animal models have revealed synchronized changes to both the subchondral bone and the articular cartilage during the development to OA (Botter et al., 2009; Stok et al., 2009) meaning that the changes occur concurrently.

In another animal model involving medial meniscectomy and medial collateral ligament (MCL) transaction, established by Zhang et al. (2012), analyses of the dysregulated genes indicated that the events underlying subchondral bone remodeling occurred sequentially and in a time-dependent manner at the gene expression level. The reported immunohistochemistry and real-time PCR analyses in this study strongly support the hypothesis that remarkable changes occur in the subchondral bone and precede significant articular cartilage degeneration.

MRI examinations have demonstrated increased tibial plateau size and involvement of the subchondral bone already at the preradiographic OA stage (Reichenbach et al., 2008; Dore et al., 2010; Roemer et al., 2010).

Different observations have also been made in cartilage content. Liu et al. (2003) for example found differences in proteoglycan levels between ACL and spontaneous OA models.

In the past especially controversial results have been reported with regard to the regulation of aggrecan. While Young et al. (2005) found an upregulation, Lorenz et al. (2005) did not find a change in aggrecan levels, Kapoor et al. (2011) even saw a down regulation in advanced osteoarthritis as aggrecan is degraded by both aggrecanes and MMPs. Notably, aggrecan content decreased in spontaneous OA models, but increased after previous ACL transection.

Marijnissen et al. (2002) found that a groove model led to greater cartilage damage but less synovial inflammation compared to an ACL model.

These results show that OA progression can vary, depending on the type of impact. Therefore the method used to induce cartilage changes needs to be carefully considered, and generalization of results to humans in vivo should be done cautiously. An important point in this context is that expression as measured by RNA in real time PCR should not be considered as a mean of absolute quantification of cartilage composition, but the relative changes in collagen and aggrecan mRNA levels can be regarded as an index of chondrocyte response to joint damage, although these mRNA levels parallel remarkably the reported changes in aggrecan, proteoglycan and collagen biosynthesis (Lorenz et al. 2005).

However, already under physiological conditions not only a mechanical interaction of the mineralized subchondral tissues with articular cartilage exists. This was demonstrated for example by Pan et al. (2009) using a sodium fluorescein tracer and photobleaching technique to measure the permeability of the interface between bone and cartilage in the knee joint of rats. Using a murine model, the same group of Pan et al. (2012) showed that both cartilage damage and vascular invasion can increase the number and size of these naturally occurring pathways to enable crosstalk between bone and cartilage via diffusion of small molecules.

Several authors, e.g. Cox et al. (2012) and Bobinac et al. (2003) reported a decreasing Bone Volume Fraction with increasing distance from healthy cartilage. It can be postulated now that, with advancing osteoarthritis, the decline in the Bone Volume Fraction with increasing depth level seems to become more pronounced compared to osteochondral samples from healthy controls. Consequently, the possibility of a biochemical signalling from the degenerating cartilage via the synovial fluid as posted by Cox et al. (2012) may indeed explain the depth-dependency of the bone changes. This group furthermore found Bone Volume Fraction and bone matrix mineralization, assessed as Bone Tissue Mineral Density (TMD), to be negatively correlated and considered a mechanoregulated bone adaptation.

Bone-cartilage crosstalk via subchondral pores in non-diseased joints, cellular signalling via microcracks caused, for example, by repetitive loading, and increased bone remodelling caused by vascular invasion stimulated by elevation of angiogenic factors in the synovial fluid, such as vascular endothelial growth factor are in the focus of further investigation to determine how interaction at the cellular level changes biomechanical characteristics in vivo and what forthcoming experimental treatment strategies might include.

References

Akiyama K., Sakai T., Sugimoto N., Yoshikawa H and Sugamoto K. (2012). Three-dimensional distribution of articular cartilage thickness in the elderly talus and calcaneus analyzing the subchondral bone plate density. Osteoarthritis Cartilage 20, 296-304.

Baelde H.J., Cleton-Jansen A.M., van Beerendonk H., Namba M., Bovee J.V.M.G. and Hogendoorn P.C.W. (2001). High Quality RNA isolation from tumours with low cellularity and high extracellular matrix component for cDNA microarrays: application to chondrosarcoma. J. Clin. Pathol. 54, 778-782.

Bobinac D., Spanjol J., Zoricic S. and Maric I. (2003). Changes in articular cartilage and subchondral bone histomorphometry in osteoarthritic knee joints in humans. Bone 32, 284-290.

Botter S.M., Glasson S.S., Hopkins B., Clockaerts S., Weinans H., van Leeuwen J.P. and van Osch G.J. (2009). ADAMTS5-/- mice have less subchondral bone changes after induction of osteoarthritis through surgical instability: implications for a link between cartilage and subchondral bone changes. Osteoarthritis Cartilage 17, 636-645.

Burger C., Mueller M., Wlodarczyk P., Goost H., Tolba R.H., Rangger C., Kabir K. and Weber O. (2007). The sheep as a knee osteoarthritis model: early cartilage changes after meniscus injury and repair. Lab. Anim. 41, 420-431.

Burr D.B. and Gallant M.A. (2012). Bone remodelling in osteoarthritis. Nat. Rev. Rheumatol. 8, 665-673

Cox L.G., van Donkelaar C.C., van Rietbergen B., Emans P.J. and Ito K. (2012). Decreased bone tissue mineralization can partly explain subchondral sclerosis observed in osteoarthritis. Bone 50, 1152-1161.

Ding M., Odgaard A., Danielsen C.C. and Hvid I. (2002). Mutual associations among microstructural, physical and mechanical properties of human cancellous bone. J. Bone Joint Surg. Br. 84, 900- 907.

Ding M., Odgaard A. and Hvid I. (2003). Changes in the three-dimensional microstructure of human tibial cancellous bone in early osteoarthritis. J. Bone Joint Surg. Br. 85, 906-912.

Dore D., Quinn S., Ding C., Winzenberg, T., Cicuttini F. and Jones G. (2010). Subchondral bone and cartilage damage: a prospective study in older adults. Arthritis Rheum. 62, 1967-1973.

Duncan H., Jundt J., Riddle J.M., Pitchford W. and Christopherson T. (1987). The tibial subchondral plate. A scanning electron microscopic study. J. Bone Joint Surg. Am. 69, 1212-1220

Ehrlich M.G., Armstrong A.L., Treadwell B.V. and Mankin H.J. (1986). Degradative enzyme systems in cartilage. Clin. Orthop. Relat. Res. 213, 62-68.

Goulet R.W., Goldstein S.A., Ciarelli M.J., Kuhn J.L., Brown M.B. and Feldkamp L.A. (1994). The relationship between the structural and orthogonal compressive properties oftrabecular bone. J. Biomech. 27, 375-389.

Hildebrand T. and Ruegsegger P. (1997). A new method for the model-independentassessment of thickness in three-dimensional images. J. Microsc. 185, 67.

Kapoor M., Martel-Pelletier J., Lajeunesse D., Pelletier J.P. and Fahmi H. (2011). Role of proinflammatory cytokines in the pathophysiology of osteoarthritis. Nat. Rev. Rheumatol. 7, 33-42.

Kempson G.E., Muir H., Pollard C. and Tuke M. (1973). The tensile properties of the cartilage of human femoral condyles related to the content of collagen and glycosaminoglycans. Biochem. Biophys. Acta 297, 456-472.

Lahm A., Kreuz P. C., Oberst M., Haberstroh J., Uhl M. and Maier D. (2006). Subchondral bone remodeling after experimental subchondral fractures of the knee joint with secondary osteoarthritis. Arch. Orthop. Trauma Surg. 126, 582-587.

Liu W., Burton-Wurster N., Glant T.T., Tashman S., Sumner D.R., Kamath R.V., Lust G., Kimura J.H. and Cs-Szabo G. (2003). Spontaneous and experimental osteoarthritis in dog: similarities and differences in proteoglycan levels. J. Orthop. Res. 21, 730-737.

Lorenz H., Wenz W., Ivancic M., Steck E. and Richter W. (2005). Early and stable upregulation of collagen type II, collagen type I and YKL40 expression levels in cartilage during early experimental osteoarthritis occurs independent of joint location and histological grading. Arthritis Res. Ther. 7, 156-165.

Marijnissen A.C., van Roermund P.M., Verzijl N., Tekoppele J.M., Bijlsma J.W., Lafeber F.P. (2002). Steady progression of osteoarthritic features in the canine groove model. Osteoarthritis Cartilage 10, 282-289.

Miosge N., Hartmann M., Maelicke C. and Herken R. (2004). Expression of collagen type I and type II in consecutive stages of human osteoarthritis. Histochem. Cell. Biol. 122, 229-236.

Pan J., Zhou X., Li W., Novotny J.E., Doty S.B. and Wang L. (2009). In situ measurement of transport between subchondral bone and articular cartilage. J. Orthop. Res. 27, 1347-1352.

Pan J., Wang B., Li W., Zhou X., Scherr T., Yang Y., Price C. and Wang L. (2012). Elevated cross-talk between subchondral bone and cartilage in osteoarthritic joints. Bone 51, 212-217.

Panula H.E., Nieminen J., Parkkinen J.J., Arnala I., Kröger H. and Alhava E. (1998) Subchondral bone remodelling increases in early experimental osteoarthritis in young Beagle dogs. Acta Orthop. Scand. 69, 627-632

Quasnichka H.L., Anderson-MacKenzie J.M. and Bailey A.J. (2006). Subchondral bone and ligament changes precede cartilage degradation in guinea pig osteoarthritis. Biorheology 43, 389-397.

Radin E.L. and Rose R.M. (1986). Role of subchondral bone in the initiation and progression of cartilage damage. Clin. Orthop. Rel. Res. 213, 34-40.

Raudenbush D., Sumner D.R., Panchal P.M., Muehleman C. (2003) Subchondral thickness does not vary with cartilage degeneration on the metatarsal. J. Am. Podiatr. Med. Assoc. 93, 104-110.

Reichenbach S., Guermazi A., Niu J., Neogi T., Hunter D.J., Roemer F.W., McLennan C.E., Hernandez-Molina G. and Felson D.T. (2008). Prevalence of bone attrition on knee radiographs and MRI in a community-based cohort. Osteoarthritis Cartilage 16, 1005-1010.

Roemer F.W., Neogi T., Nevitt M.C., Felson D.T., Zhu Y., Zhang Y., Lynch J.A., Javaid M.K., Crema M.D., Torner J., Lewis C.E. and Guermazi A. (2010). Subchondral bone marrow lesions are highly associated with, and predict subchondral bone attrition longitudinally: the MOST study. Osteoarthritis Cartilage 18, 47-53.

Ruettger A., Neumann S., Wiederanders B. and Huber R. (2010). Comparison of different methods for preparation and characterization of total RNA from cartilage samples to uncover osteoarthritis in vivo. BMC Res. Notes. 3, 7.

Sniekers Y.H., Interna F., Lafeber F.P., van Osch G.J., van Leeuwen J.P., Weinans H. and Mastbergen S.C. (2008). A role for subchondral bone changes in the process of osteoarthritis; a micro-CT study of two canine models. BME Musculoskelet. Disord. 9, 20.

Sokolove J. and Lepus C.M. (2013). Role of inflammation in the pathogenesis of osteoarthritis: latest findings and interpretations. Ther. Adv. Musculoskelet. Dis. 5, 77-94.

Stok K.S., Pelled G., Zilberman Y., Kallai I., Goldhahn J., Gazit D. and Müller R. (2009). Revealing the interplay of bone and cartilage in osteoarthritis through multimodal imaging of murine joints. Bone 45, 414-422.

Thomsen J.S., Laib A., Koller B., Prohaska S., Mosekilde L. and Gowin W. (2005) Stereological measures of trabecular bone structure: comparison of 3D micro computed tomography with 2D histological sections in human proximal tibial bone biopsies. J. Microsc. 218, 171-179.

Vandesompele J., De Preter K., Pattyn F., Poppe B., Van Roy N., De Paepe A. and Speleman F. (2002). Accurate normalization of realtime quantitative RT-PCR data by geometric averaging of

multiple internal control genes. Genome Biol. 3, 7.

Young A.A., Smith M.M., Smith S.M., Cake M.A., Ghosh P., Read R.A., Melrose J., Sonnabend D.H., Roughley P.J. and Little C.B. (2005). Regional assessment of articular cartilage gene expression and small proteoglycan metabolism in an animal model of osteoarthritis. Arthritis Res. Ther. 7, 852-861.

Zhang L., Hu H., Tian F., Song H. and Zhang Y. (2011). Enhancement of subchondral bone quality by alendronate administration for the reduction of cartilage degeneration in the early phase of experimental osteoarthritis. Clin. Exp. Med. 11, 235-243.

Zhang R., Fang H., Chen Y., Shen J., Lu H., Zeng C., Ren J., Zeng H., Li Z., Chen S., Cai D. and Zhao Q. (2012). Gene expression analyses of subchondral bone in early experimental osteoarthritis by microarray. PLoS One 7, e32356.

Accepted May 14, 2014